Journal of Visualization, Vol. 10, No. 2 (2007)179-186

Regular Paper

Numerical Simulation of Flow around a Circular Cylinder with Curved Sectional Grooves

Yamagishi, Y.*[1] and Oki, M.*[2]

*1 Department of Mechanical Engineering, Kanagawa Institute of Technology, 1030 Shimoogino, Atugi-shi, Kanagawa 243-0292, Japan. E-mail: yamagisi@me.kanagawa-it.ac.jp
*2 School of High-Technology for Human Welfare, Tokai University, 317 Nishino, Numazu-shi, Shizuoka 410-0395, Japan.

Received 14 October 2006
Revised 9 February 2007

Abstract : In a circular cylinder with uniform flow, a sudden decrease in the drag force occurs at a high Reynolds numbers; however, it is known that the same phenomenon occurs at a lower Reynolds number in the case where there exist grooves or roughness on the circular cylinder surface. To clarify the flow characteristics around a circular cylinder in the case of changing the shape of grooves we analyzed the drag coefficient, lift coefficient, turbulent kinetic energy, vorticity and pressure by applying the RNG $k-\varepsilon$ turbulent model. The shapes of the grooves were arced, triangulated and curved. The results showed that the separation point for a circular cylinder with curved sectional grooves shifts to the most downstream side and the drag coefficient becomes the smallest among circular cylinders with grooves.

Keywords : Circular Cylinder with Grooves, Curved Sectional Grooves, Flow Characteristics, Drag Coefficient, Numerical Visualization.

1. Introduction

In the case of a circular cylinder with uniform flow, a sudden decrease in the drag force occurs at a high Reynolds number Re = 3 x 10^5; however, it is known that the same phenomenon occurs at a lower Reynolds number in the case where there exist grooves or roughness on the circular cylinder surface. Such a drag reduction phenomenon can be applied to vessels, airplanes and electricity lines for example, to improve energy efficiency, or to reduce wind load. A circular cylinder with roughness was examined experimentally (Achenbach et al., 1971 and 1981; Adachi et al., 1989). A circular cylinder with grooves was examined (Kimura et al., 1991; Lee et al., 1996; Oki et al., 1994 and 1999; Takayama et al., 2005; Yamagishi et al., 2005-1). A flat plate and a sphere with grooves were examined (Aoki et al., 2000 and 2003).

Recently, we clarified that the drag coefficient of a circular cylinder with triangular grooves decreases by about 11 % compared with circular cylinder with arc grooves and about 33 % compared with smooth cylinder (Yamagishi et al., 2004). Moreover, the mechanism of the drag decrease was also clarified. The separation bubble becomes smaller in the triangular groove since the geometrical space of a triangular groove is smaller than that of an arc groove. Therefore, the large value of the turbulent kinetic energy of a circular cylinder with triangular grooves adheres to the surface of the cylinder from the upstream to the downstream side. So the separation point of the circular cylinder with triangular grooves shifts towards the downstream side since the convex part of the velocity becomes larger compared with that in the circular cylinder with arc grooves in the boundary layer

(Yamagishi et al., 2005). This study aimed to investigate the shape of the groove that becomes smaller than the drag for triangular grooves based on the mechanism of drag decrease.

2. Numerical Analysis

2.1 Analytic Model

Figure 1(a) shows the circular cylinder with grooves used for this study; it is 48 mm in diameter. Grooves of 3.7 mm width and 0.5 mm depth were attached to the surface of each cylinder at intervals of 11.25° in the vertical direction, and the number of grooves was 32. Figure 1(b)-1) shows an arc groove (Model A). Figure 1(b)-2) shows a triangular groove (Model B). Figure 1(b)-3) shows the curved sectional shape I (Model C) which had the corners of triangular groove rounded with a 1 mm radius. Figure 1(b)-4) shows curved sectional shape II (Model D) which had the sides of model C rounded with a 4.5mm radius to reduce the region of separation bubbles in the grooves.

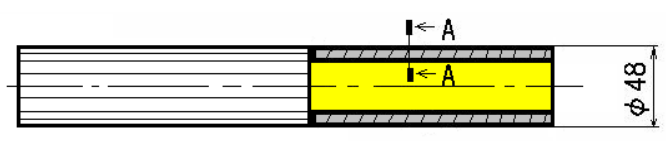

(a) Circular cylinder with grooves [Unit : mm]

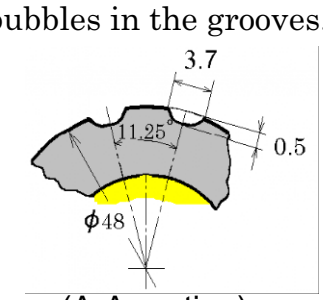

(A-A section)

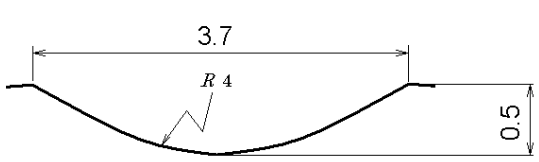

1) Arc (Model A)

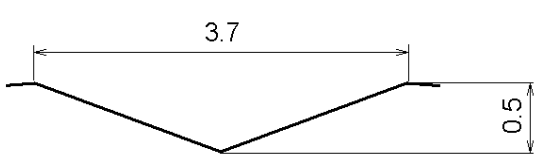

2) Triangle (Model B)

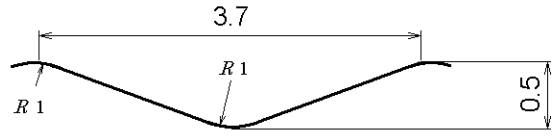

3) Curved sectional shape I (Model C)

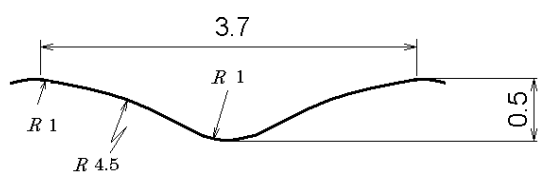

4) Curved sectional shape II (Model D)

(b) Sectional shapes of grooves [Unit : mm]

Fig. 1. Circular cylinder with grooves.

2.2 Analytic Method

Numerical analysis was performed using a versatile fluid analysis software package Fluent 6.2. Analyses were made in an unsteady two-dimensional turbulent flow. The RNG k–ε model was used as the turbulent model. Whole meshes of the analytic region and meshes near the circular cylinder surface are shown in Fig. 2. The boundary conditions are listed in Table 1.

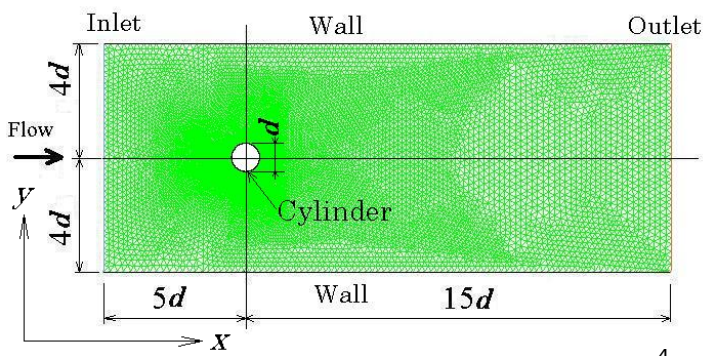

(a) Whole meshes (Grid number = 8 x 10^4)

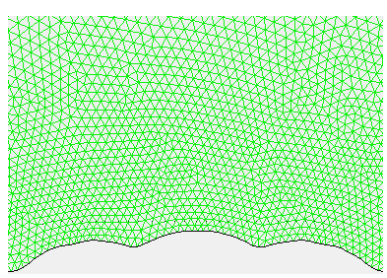

(b) Meshes near the circular cylinder surface

Fig. 2. Whole meshes and meshes near the Model D surface.

Table 1. Boundary conditions.

Cylinder surface and wall	u=0, v=0
Inlet	u=U, v=0
	Turbulence intensity=0.65%
Outlet	p_{out} =0

u : Velocity component in the x direction
v : Velocity component in the y direction
U : Uniform flow velocity
p_{out} : Outlet pressure

3. Results and Discussion

3.1 Drag Property

Figure 3 shows the variations in the drag coefficients C_D with Reynolds number Re for Model A (●), B (▲), C (■) and D (▼) by numerical analysis. Experimental results of Model A (○), B (Δ) and a smooth cylinder (□) by drag measurements are shown in this figure. The drag measurements were obtained by a wake traverse method based on momentum theory (Yamagishi et al. , 2003, 2004 and 2005). The results of numerical analysis were carried out the time average of the results of unsteady analysis.

For comparison, the measurements on a smooth cylinder (-----) are also included (Wieselsberger, 1921). From this figure, the experimental value for the smooth cylinder (-□-) agrees with the measurement of Wieselsberger in the range of Reynolds numbers Re = 1 x 10^4 ~ 10 x 10^4. It is clear that the appropriateness of this drag measurement was proven. The results of numerical analysis of Models A (●) and B (▲) show a tendency to agree well with the experimental values (○ and Δ). It is clear that appropriateness of this numerical analysis was proven. The drag coefficients of Models C and D were then calculated using the same numerical analysis method.

Curve of the drag coefficient can be divided into subcritical, critical, supercritical and transcritical region. There is no difference in change of the drag coefficient in respect to the shapes of the grooves in the range of the critical region from the subcritical region (Re = 1 x 10^4 ~ 3 x 10^4). But the drag coefficient becomes small in the order of Models A, B, C and D in the range of the transcritical region (Re = 5 x 10^4 ~ 10 x 10^4). It is clear that the drag coefficient C_D for Model D (▼) decreases by about 20 % compared with that for Model A (●), and about 40 % compared with the smooth cylinder(□).

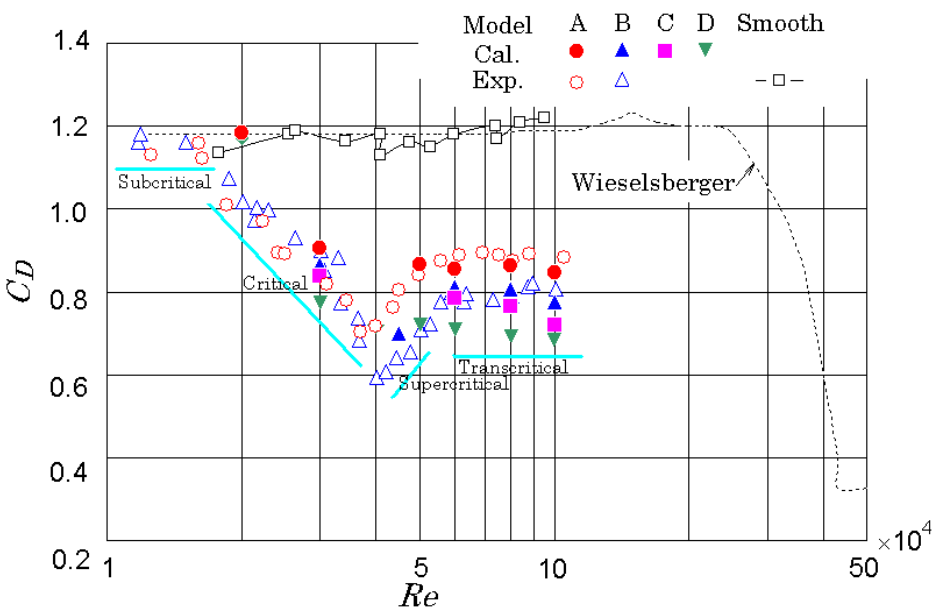

Fig. 3. Drag coefficients.

3.2 Separation Point

The computational results of the streamlines near the surface of the circular cylinder with grooves at Re =10 x 10^4 are shown in Figs. 4(a), (b), (c) and (d), which show streamlines from θ = 90° to the downstream side (θ : angle from the stagnation point). The flow is from left to right. The separation points of Models A and B occur at the corner, although the separation points of Models C and D shift toward the downstream side since the corner is rounded. The separation bubble becomes smaller in the groove of Model D since the geometrical space of Model D is smaller than those of the others. The separation point shifts towards the downstream side in the order of Models A, B, C and D.

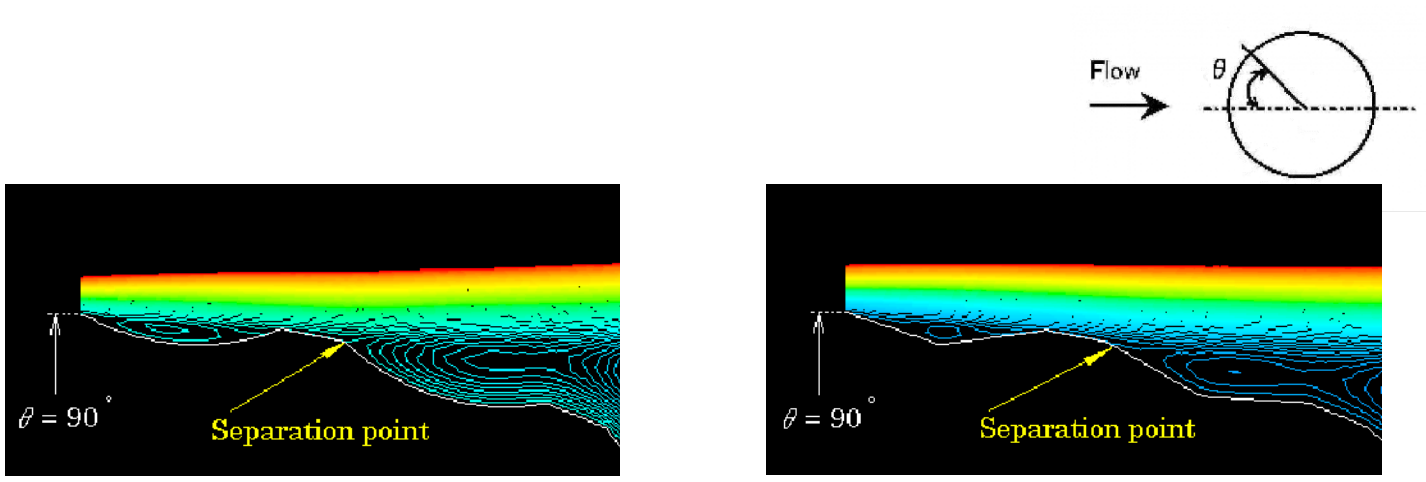

(a) Model A (b) Model B

(c) Model C (d) Model D

Fig. 4. Streamlines near the circular cylinders with grooves (Re = 10 x 10^4).

The computational results of the turbulent kinetic energy distributions near Models A and D surfaces at Re = 10 x 10^4 are shown in Figs. 5(a) and (b), respectively. The flow is from left to right.

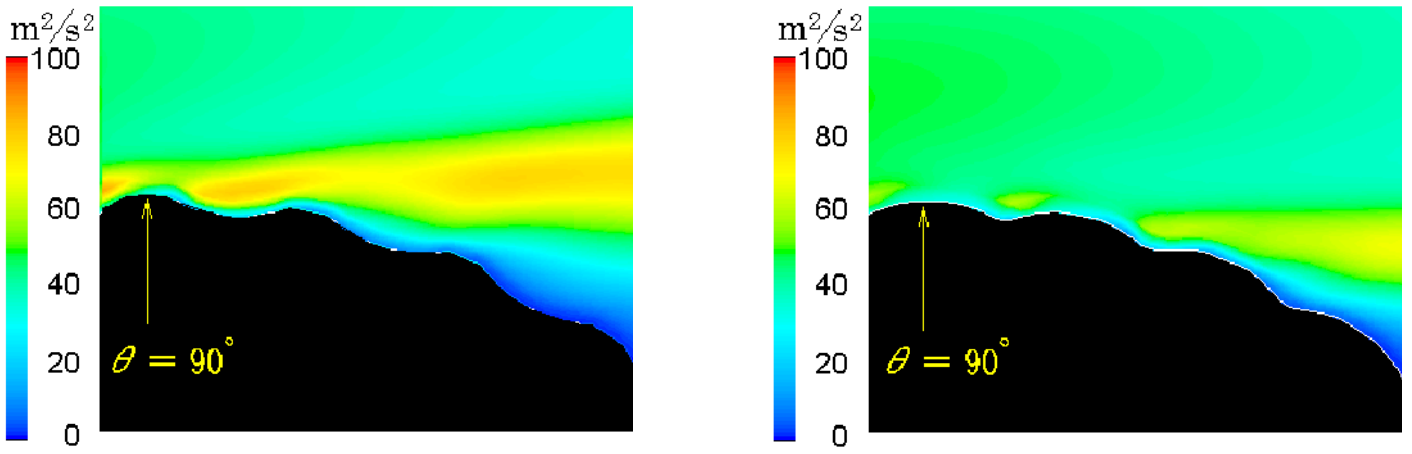

(a) Model A (b) Model D

Fig. 5. Turbulent kinetic energy distribution near the circular cylinders with grooves (Re = 10 x 10^4).

This figure shows the turbulent kinetic energy distributions from $\theta = 90°$ to the downstream side. Since the separation bubbles become smaller in the grooves of Model D, the position of reattachment for Model D is inside the groove compared with Model A. Therefore, the large value of the turbulent kinetic energy of Model D adheres to the surface of the cylinder from the upstream to the downstream side. Thus the separation point of Model D shifts towards the downstream side and the drag coefficient is small.

The computational results of the vorticity distributions near Models A and D surfaces at $Re = 10 \times 10^4$ are shown in Figs. 6(a) and (b), respectively. The flow is from left to right. The red range of the activity of the generating vortex exists near the surface of Model D from the upstream to the downstream side. We found that partial separation and reattachment are repeated in the range shown in red and that separation occurs beyond the range shown in red.

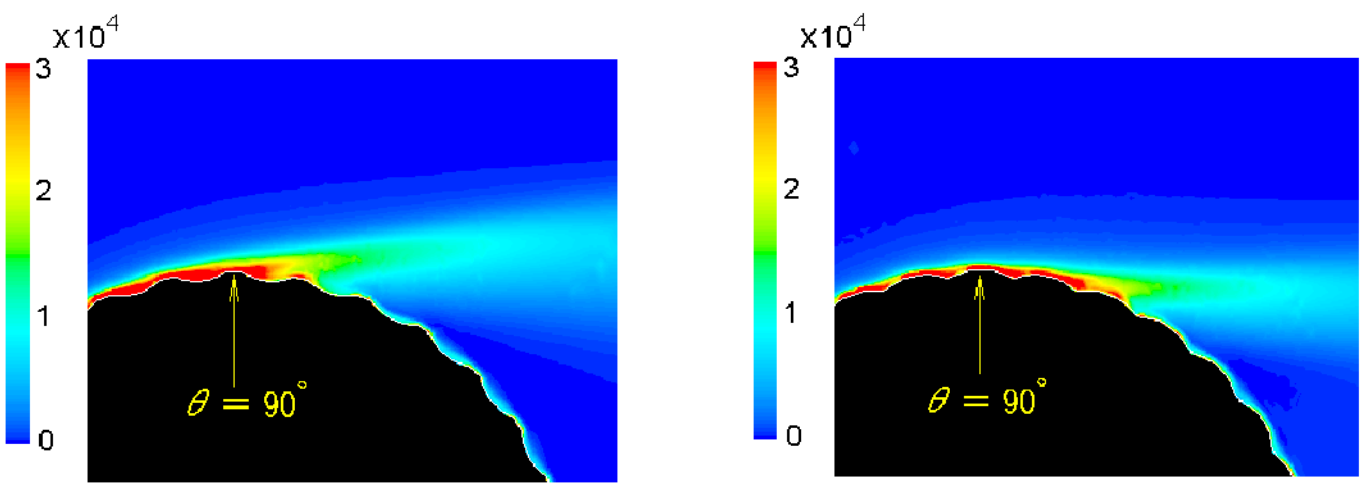

(a) Model A (b) Model D

Fig. 6. The vorticity distribution near the circular cylinders with grooves (Re = 10 x 10^4).

The computational results of the pressure distributions on Models A and D surfaces at $Re = 10 \times 10^4$ are shown in Fig. 7. And the experimental results of Model A are shown too. The ordinate shows the pressure coefficients C_p and the abscissa shows the angle θ from the forward stagnation point. The positions of separation point are shown. The backpressure coefficient C_{pb} for Model D becomes larger compared with that for Model A. The positions of the grooves are shown in the lower part of this figure. The pressure distribution of Model A is sharp at the corner of grooves.

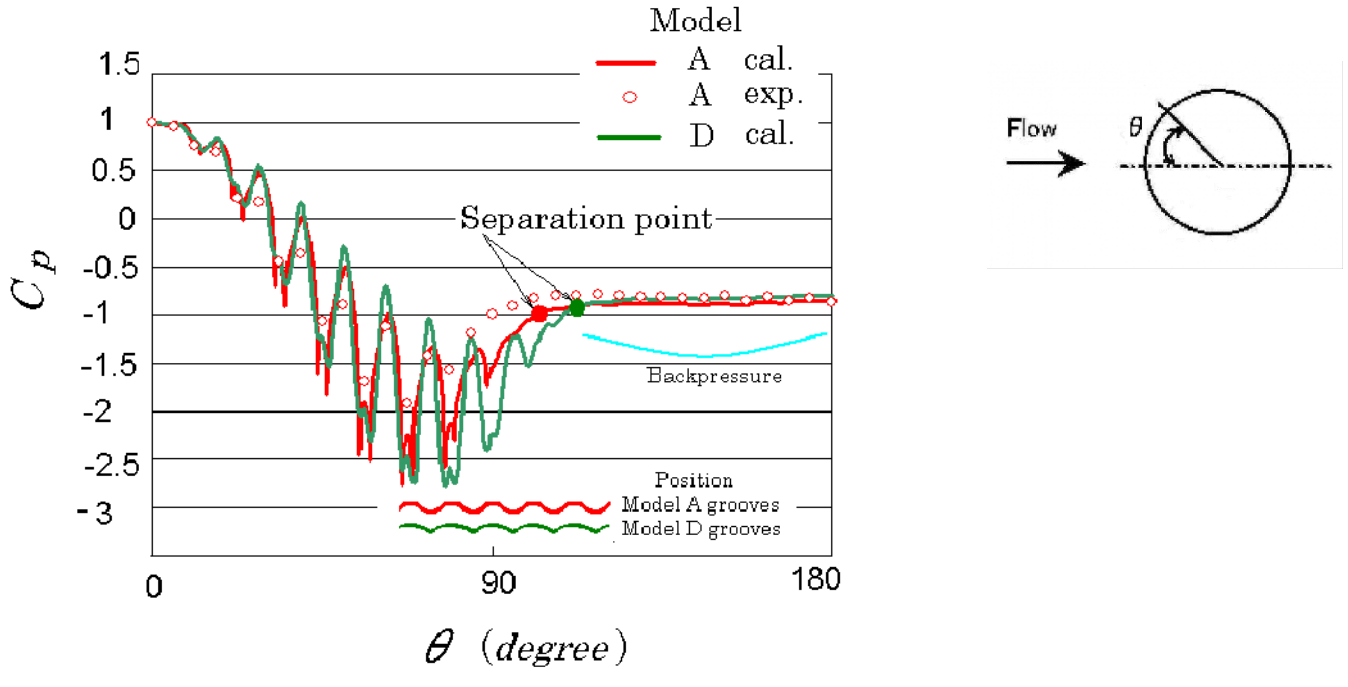

Fig. 7. Pressure distribution around the cylinder with grooves (Re = 10 x 10^4).

Figure 8 shows the computational results of the variations in the velocity gradient $(du/dy)_{y=surface}$ on the surface of a cylinder with an angle θ from the stagnation point at Re = 10 x 10^4. The angles θ of the grooves are shown on the right side of Fig. 8. The position of the velocity gradient $(du/dy)_{y=surface}$ = 0 corresponds to the position of partial separation or reattachment. The velocity gradient $(du/dy)_{y=surface} < 0$ corresponds to the reverse flow. The velocity gradient $(du/dy)_{y=surfacee} > 0$ corresponds to the attached flow. For the circular cylinder with grooves, the partial separation and reattachment is repeated by the effects of the grooves; so that the separation for Model A occurs at about θ = 102°, Model B at about θ = 103°, Model C at about θ = 104°, and Model D at about θ = 112°.

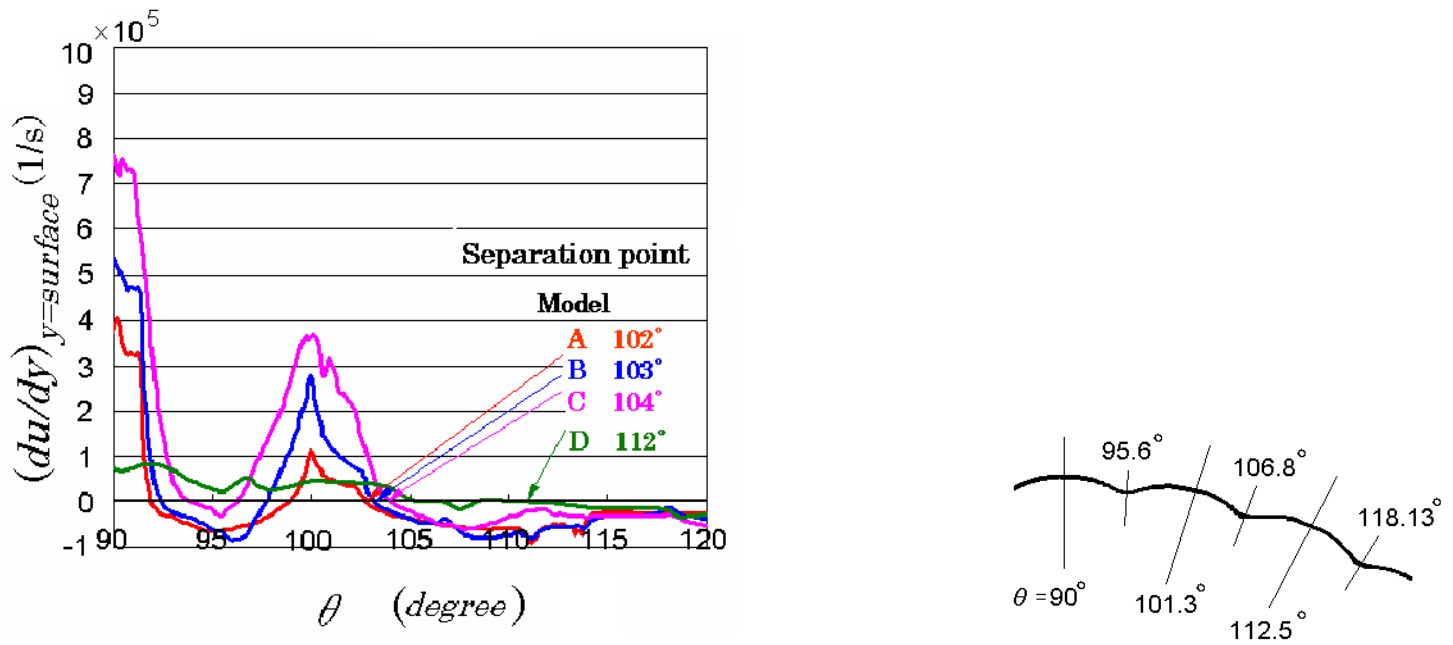

Fig. 8. Velocity gradient around circular cylinders with grooves (Re = 10 x 10^4).

3.3 Lift Property

The computational results of the vorticity distributions behind Models A and D at Re = 10 x 10^4 are shown in Figs. 9(a) and (b), respectively. The flow is from left to right. It is clear that the value of vorticity and the region of wake for Model D become smaller compared with that for Model A since the position of separation point becomes downstream side.

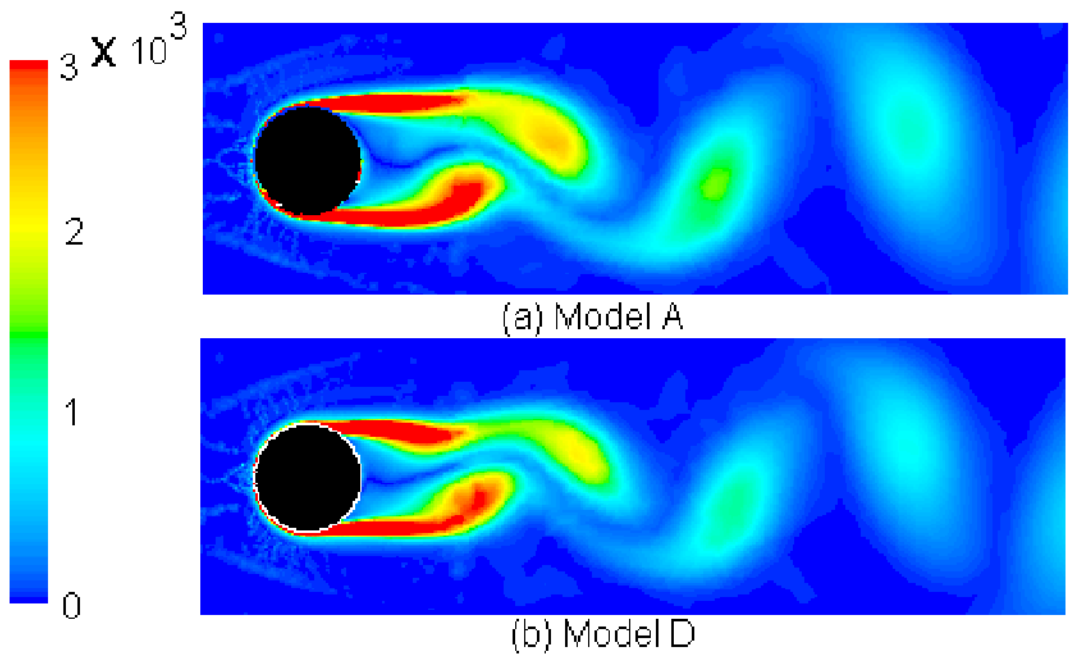

Fig. 9. Vorticity distribution behind circular cylinders with grooves (Re = 10 x 10^4).

Figure 10 shows the numerical results of the fluctuation of the lift coefficient C_L at $Re = 10 \times 10^4$. The abscissa shows non-dimensional time t^* ($t^* = t/(d/U)$, t : time, d : diameter of the circular cylinder, and U : uniform velocity) and the ordinate shows C_L. It is clear that the amplitude and period of the fluctuation of lift coefficient for Model D become smaller compared with those for Model A.

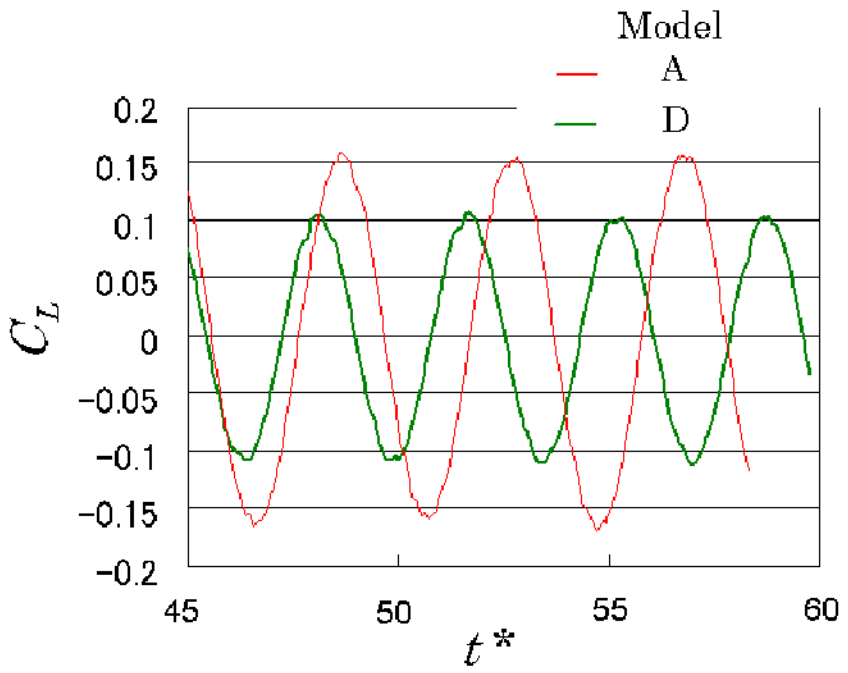

Fig. 10. Time history of lift coefficient (Re = 10 x 10^4).

Figure 11 shows the variations in Strouhal number St with Reynolds number Re for Models A and D. The results of numerical analysis of Model A show a tendency to agree well with experimental values. The frequency of the generating vortex f is calculated from the fluctuation of the lift coefficient. The frequency of Model A is f =163 and that of Model D is f =181. Therefore, Strouhal number St ($St = fd/U$, f: frequency, d : diameter of the circular cylinder, and U : uniform velocity) of Model A is $St = 0.249$ and that of Model D is $St = 0.276$. It is clear that the drag coefficient of Model D becomes small compared with that of Model A, since the Strouhal number of Model D becomes larger compared with that of Model A.

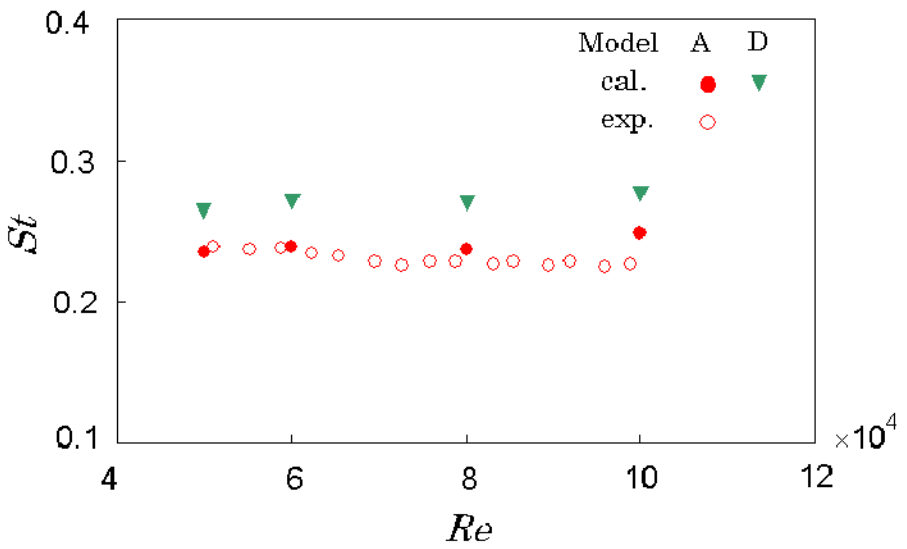

Fig. 11. Strouhal vs. Reynolds numbers.

4. Conclusion

The results of this study lead to the following conclusions:

(1) The separation points of Models A and B occur at the corner, although the separation points of Models C and D shift toward the downstream side since the corner is rounded and the separation bubbles becomes smaller in the grooves of Model D since the region of the separation babbles of Model D is smaller than those of the other grooves. The drag coefficient becomes small in the order of Models A, B, C and D in the range of transcritical region ($Re = 5 \times 10^4 \sim 10 \times 10^4$). The drag coefficient for Model D decreases by about 40% compared with a smooth cylinder.

(2) The amplitude and period of the fluctuation of the lift coefficient for Model D become smaller compared with that for Model A. The Strouhal number of Model D becomes larger compared with that of Model A in the transcritical region.

References

Achenbach, E., Influence of surface roughness on the cross-flow around a circular cylinder, Journal of Fluid Mechanics, 46-2 (1971), 321-335.

Achenbach, E. and Heinecke, E., On vortex shedding from smooth and rough cylinders in the range of Reynolds numbers $6x10^3$ to 5×10^6. Journal of Fluid Mechanics, 109 (1981), 239-251.

Adachi, T., Ono, H., Matsuuchi, K., Kawai, T. and Cho, T., Flow around a circular cylinder in the high Reynolds number range, Transactions of the Japan Society of Mechanical Engineers B, 55-511 (1989), 685-692 (in Japanese).

Aoki, K., Okanaga, H. and Nakayama, Y., Control of Boundary Layer on a Flat Plate by Means of Cavity Flow, Journal of Visualization, 3-3 (2000), 211-220.

Aoki, K., Ohike, A., Yamaguchi, K. and Nakayama, Y., Flying Characteristics and Flow Pattern of a Sphere with Dimples, Journal of Visualization, 6-1 (2003), 67-76.

Kimura, T. and Tsutahara, M., Fluid dynamic effects of grooves on circular cylinder surface, AIAA J, 29-12 (1991), 2062-2068.

Lee, S., Aoki, K., Okanaga, H. and Oki, M., The flow pattern and characteristics around a rotating circular cylinder with grooves, Proc. of the 4th Asian Symp. on Visualization (Beijing), (1996), 613-618.

Oki, M., Suehiro, M., Aoki, K. and Nakayama, Y., Effect of grooves' depth on circular cylinder, FLUCOME'94 (Toulouse), (1994), 811-816.

Oki, M., Aoki, K. and Nakayama, Y., Effect of grooves' depth for flow characteristics around a circular cylinder with grooves, Transaction of the Japan Society of Mechanical Engineering, 65-631, B (1999), 870-875 (in Japanese).

Takayama, S. and Aoki, K., Flow Characteristics around a Rotating Grooved Circular cylinder with Grooved of Different Depths, Journal of Visualization, 8-4 (2005), 295-303.

Wieselsberger, C., New Data on The Laws of Fluid Resistance, Physikalische Zeitschrift, 22 (1921), 321-328.

Yamagishi, Y. and Oki, M., Effect of Groove Shape on Flow Characteristics around a Circular Cylinder with Grooves, Journal of Visualization, 7-3 (2004), 209-216.

Yamagishi, Y. and Oki, M., Effect of Number of Grooves on Flow Characteristics around a Circular Cylinder with Triangular Grooves, Journal of Visualization, 8-1(2005-1), 57-64.

Yamagishi, Y. and Oki, M., Effect of Grooves Shape on Drag Coefficient of a Circular Cylinder with Grooves, Journal of Japan Society for Design Engineering, 40-10 (2005-10), 527-533 (in Japanese).

Author Profile

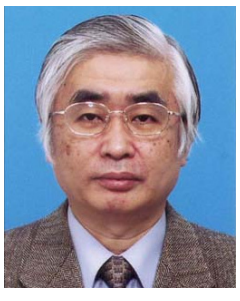

Yoichi Yamagishi : He received his M.Sc. (Eng.) degree in Mechanical Engineering in 1978 from Tokai University and his Ph.D. in Mechanical Engineering in 2006 from the same university. After obtaining M.Sc. he worked as an engineer at Hibiya Engineering, Ltd. He then became an assistant professor of Kanagawa Institute of Technology.

Makoto Oki: He received his M.Sc. (Eng.) degree in Mechanical Engineering in 1976 from Tokai University and his Ph.D. in Mechanical Engineering in 2000 from the same university. After obtaining M. Sc. he worked as a system engineer at Japan Advanced Numerical Analysis, Inc.. He then became an assistant professor of Tokai University, and currently is a professor. His current research interests are computational fluid dynamics, computer graphics and internet application.